J|A|C|S
ARTICLES
Published on Web 07/22/2003

Structure of Gramicidin A in a Lipid Bilayer Environment Determined Using Molecular Dynamics Simulations and Solid-State NMR Data

Toby W. Allen,[†,‡] Olaf S. Andersen,[‡] and Benoit Roux*[,†]

Contribution from the Department of Physiology and Biophysics and Department of Biochemistry, Weill Medical College of Cornell University, New York, New York 10021

Received November 12, 2002; E-mail: Benoit.Roux@med.cornell.edu

Abstract: Two different high-resolution structures recently have been proposed for the membrane-spanning gramicidin A channel: one based on solid-state NMR experiments in oriented phospholipid bilayers (Ketchem, R. R.; Roux, B.; Cross, T. A. *Structure* **1997**, *5*, 1655−1669; Protein Data Bank, PDB:1MAG); and one based on two-dimensional NMR in detergent micelles (Townsley, L. E.; Tucker, W. A.; Sham, S.; Hinton, J. F. *Biochemistry* **2001**, *40*, 11676−11686; PDB:1JNO). Despite overall agreement, the two structures differ in peptide backbone pitch and the orientation of several side chains; in particular that of the Trp at position 9. Given the importance of the peptide backbone and Trp side chains for ion permeation, we undertook an investigation of the two structures using molecular dynamics simulation with an explicit lipid bilayer membrane, similar to the system used for the solid-state NMR experiments. Based on 0.1 μs of simulation, both backbone structures converge to a structure with 6.25 residues per turn, in agreement with X-ray scattering, and broad agreement with SS backbone NMR observables. The side chain of Trp 9 is mobile, more so than Trp 11, 13, and 15, and undergoes spontaneous transitions between the orientations in 1JNO and 1MAG. Based on empirical fitting to the NMR results, and umbrella sampling calculations, we conclude that Trp 9 spends 80% of the time in the 1JNO orientation and 20% in the 1MAG orientation. These results underscore the utility of molecular dynamics simulations in the analysis and interpretation of structural information from solid-state NMR.

Introduction

Solid-state (SS) NMR has become increasingly important for investigating the structure of membrane proteins.[1−3] In SS NMR, orientational restraints derived from anisotropic nuclear spin interactions in samples uniformly aligned with respect to the magnetic field axis are used to determine the three-dimensional molecular structure of a protein embedded in a membrane bilayer. To date, the most complete application of this technique has been the elucidation of the structure of the gramicidin A (gA) channel embedded in a lipid bilayer by Cross and co-workers.[4] This structure, which resulted from extensive experimental work with site-specific isotopic labeling, firmly established the conformation of the transmembrane ion-conducting gA channel in lipid bilayers.

To appreciate the general importance of the gA channel structure for ion permeation and for SS NMR, it is helpful to review the gA channel's contribution to the current understanding of ion permeation across membranes. The gA channel subunit has the sequence (underlined residues are D-amino acids): formyl-Val-Gly-Ala-Leu-Ala-Val-Val-Val-Trp-Leu-Trp-Leu-Trp-Leu-Trp-ethanolamine.[5] The development of a molecular perspective of channel-mediated ion permeation began about 30 years ago when Urry,[6,7] in an insightful analysis of structural models, proposed that the gA channel was a formyl-NH-terminal to formyl-NH-terminal $\beta^{6.3}$-helical dimer. According to this analysis, both left-handed (LH) and right-handed (RH) subunits were possible, though the LH structure appeared to be energetically favored. For nearly 15 years, this was the accepted gA channel structure and was widely used to interpret experimental results until 1986, when Arseniev et al.,[8] using two-dimensional solution NMR, determined that the gA structure in sodium dodecylsulfate (SDS) micelles, a membrane mimicking milieu, was an RH $\beta^{6.3}$-helical dimer (Protein Data Bank, PDB structure 1GRM [9]). Though the circular dichroism (CD) spectrum of gA in SDS was characteristic of the channel in phospholipid vesicles,[10] the relevance of this structure to that of the bilayer-spanning channel remained uncertain. These doubts were

† Department of Physiology and Biophysics, Weill Medical College of Cornell University.
‡ Department of Biochemistry, Weill Medical College of Cornell University.

(1) Davis, J. H.; Auger, M. *Prog. Nucl. Magn. Reson. Spectrosc.* **1999**, *35*, 1−84.
(2) Auger, M. *Curr. Issues Mol. Biol.* **2000**, *2*, 119−124.
(3) Marassi, F. M.; Opella, S. J. *Curr. Opin. Struct. Biol.* **1998**, *8*, 640−648.
(4) Ketchem, R. R.; Hu, W.; Cross, T. A. *Science* **1993**, *261*, 1457−1460.
(5) Sarges, R.; Witcop, B. *J. Am. Chem. Soc.* **1965**, *87*, 2011−2020.
(6) Urry, D. W. *Proc. Natl. Acad. Sci. U.S.A.* **1971**, *68*, 672−676.
(7) Urry, D. W. *Biochim. Biophys. Acta* **1972**, *265*, 115−168.
(8) Arseniev, A. S.; Lomize, A. L.; Barsukov, I. L.; Bystrov, V. F. *Biol. Membr.* **1986**, *3*, 1077−1104.
(9) Lomize, A. L.; Orekhov, V. Y.; Arseniev, A. S. *Bioorg. Khim.* **1992**, *18*, 182−200 (in Russian).
(10) Urry, D. W.; Trapane, T. L.; Prasad, K. U. *Science* **1983**, *221*, 1064−1067.

10.1021/ja029317k CCC: $25.00

dissipated in 1993 when Cross and co-workers[4] determined the structure of gA embedded in oriented dimyristoylphosphatidylcholine (DMPC) bilayers using SS NMR. Further refinement of the SS NMR in 1997[11] using a large number orientational restraints observed from specific isotopic labeling of all the residues led to a high resolution structure (PDB:1MAG). The PDB structure 1MAG is now widely employed in computational studies of ion permeation.[12−20]

A second high-resolution structure of gA in SDS micelles was determined in 2001 by Hinton and co-workers using solution NMR (PDB:1JNO).[21] Though the structures determined by solution NMR in SDS micelles and by SS NMR in DMPC bilayers are in broad agreement (both being RH $\beta^{6.3}$ helical dimers), they differ in important details: the helical pitch of the 1MAG structure is considerably higher than that of the 1JNO (and 1GRM) structures, and the orientations of several side chains are different, the most notable being the indole ring of Trp 9, which has different rotameric states.[4,21,22] Figure 1 shows how the Trp 9 side chain in the PDB:1JNO structure is splayed away from the Trp 15 side chain, whereas it is stacked on Trp 15 in the PDB:1MAG structure. Despite support for a stacked indole ring configuration from fluorescence spectroscopy,[23,24] evidence that PDB:1MAG is the predominant gA structure in the bilayer is inconclusive because SS NMR is unable to define uniquely the orientation of Trp 9.[21] The discrepancies in Trp orientation could reflect the difference between the environments presented by a detergent micelle and a phospholipid bilayer, although that is unlikely in light of the very similar CD spectra which are dominated by the Trp chromophores.[25] Alternatively, the discrepancies could arise from the different computational methodologies used to convert the spectroscopic data into 3D models. While both structures have been refined using molecular mechanical force fields and energy penalty functions representing the structural constraints, the solution NMR structure was determined from distance restraints from nuclear Overhauser effect spectroscopy (NOESY) data,[21] whereas the SS structure was determined from orientational restraints.[11]

The precision of the backbone in the refined SS NMR structure has been reported to be on the order of 0.11 Å,[26] yielding one of the highest resolutions for a membrane-bound polypeptide. By comparison, the accuracy of high quality solution NMR structures, depending on the number of restraints (NOE, J-coupling, chemical shift), is comparable to that of X-ray structures determined to 1.5−2.5 Å resolution.[27] The difference in precision is striking. Moreover, because they correspond to first-order average Hamiltonian quantities, the orientational restraints of SS NMR extracted from observed chemical shift anisotropy (CSA), dipolar coupling (DC), and deuterium quadrupolar splitting (DQS) are easily amenable to a direct structural interpretation. In contrast, the distance restraints of solution NMR are deduced from nuclear Overhauser effect (NOE), which corresponds to a second-order relaxation process.

First-order orientational restraints do, indeed, allow for generating more accurate and precise structures. For example, orientational restraints extracted from residual dipolar couplings measured on partially oriented protein samples, a method recently introduced in solution NMR, allow for more precise protein structure determination.[28] Consequently, the structural differences between the 1MAG and the 1JNO structures could arise either from differences in the membrane/micelle environments or by the lack of precision of the solution NMR structure. In this context, the gA channel is quite unique. For the past decade, it has served as one of the model systems of choice for developing and testing SS NMR techniques. Being virtually alone in its category, the precision of the 1MAG structure is assessed by considering the convergence of the Monte Carlo energy minimization structural refinement by varying the

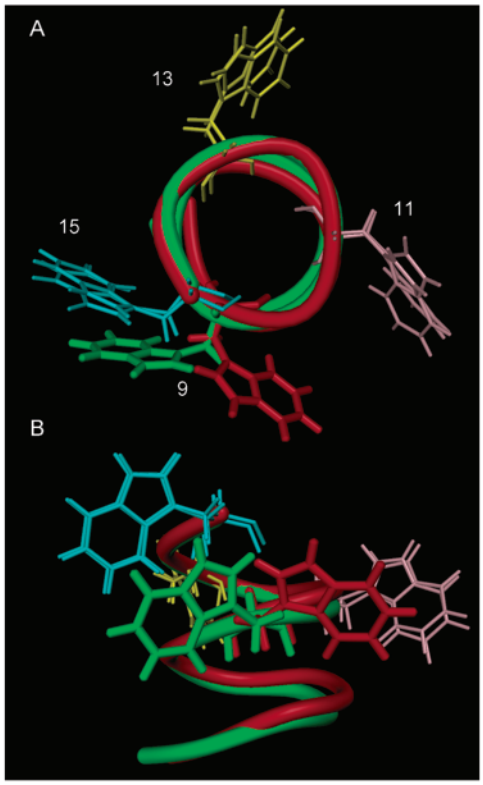

Figure 1. Gramicidin A structures: (A) One subunit of the gA channel is viewed along the *z*-axis with PDB:1JNO (red) and PDB:1MAG (green) structures superimposed after alignment to Trp 11 (pink), 13 (yellow), and 15 (cyan) side chains. (B) One subunit is viewed from the side, with the Trp residues highlighted as in structure A.

(11) Ketchem, R. R.; Roux, B.; Cross, T. A. *Structure* **1997**, *5*, 1655−1669.
(12) Chiu, S. W.; Subramaniam, S.; Jakobsson, E. *Biophys. J.* **1999**, *76*, 1929−1938.
(13) Chiu, S. W.; Subramaniam, S.; Jakobsson, E. *Biophys. J.* **1999**, *76*, 1939−1950.
(14) Kurnikova, M. G.; Coalson, R. D.; Graf, P.; Nitzan, A. *Biophys. J.* **1999**, *76*, 642−656.
(15) Tang, Y. Z.; Chen, W. Z.; Wang, C. X. *Eur. Biophys. J.* **2000**, *29*, 523−534.
(16) Hollerbach, U.; Chen, D. P.; Busath, D. D.; Eisenberg, B. *Langmuir* **2000**, *16*, 5509−5514.
(17) Cardenas, A. E.; Coalson, R. D.; Kurnikova, M. G. *Biophys. J.* **2000**, *79*, 80−93.
(18) Anderson, D. G.; Shirts, R. B.; Cross, T. A.; Busath, D. D. *Biophys. J.* **2001**, *81*, 1255−1264.
(19) de Groot, B. L.; Tieleman, D. P.; Pohl, P.; Grubmüller, H. *Biophys. J.* **2002**, *82*, 2934−2942.
(20) Edwards, S.; Corry, B.; Kuyucak, S.; Chung, S. H. *Biophys. J.* **2002**, *83*, 1348−1360.
(21) Townsley, L. E.; Tucker, W. A.; Sham, S.; Hinton, J. F. *Biochemistry* **2001**, *40*, 11676−11686.
(22) Koeppe, R. E.; Killian, J. A.; Greathouse, D. V. *Biophys. J.* **1994**, *66*, 14−24.
(23) Mukherjee, S.; Chattopadhyay, A. *Biochemistry* **1994**, *33*, 5089−5097.
(24) Scarlata, S. F. *Biophys. J.* **1988**, *54*, 1149−1157.
(25) Koeppe, R. E., II; Providence, L. L.; Greathouse, D. V.; Heitz, F.; Trudelle, Y.; Purdie, N.; Andersen, O. S. *Proteins* **1992**, *12*, 49−62.
(26) Kim, S.; Quine, J. R.; Cross, T. A. *J. Am. Chem. Soc.* **2001**, *123*, 7292−7298.
(27) Clore, G. M.; Gronenborn, A. M. *J. Mol. Biol.* **1991**, *221*, 47−53.
(28) Tolman, J. R.; Al-Hashimi, H. M.; Kay, L. E.; Prestegard, J. H. *J. Am. Chem. Soc.* **2001**, *123*, 1416−1424.

strength assigned to the penalty function;[26] a procedure that has not been verified independently. In contrast, there is a vast experience with structure determination by solution NMR, and the overall accuracy of the approach has been established by comparing with proteins of known crystallographic X-ray structure. In the absence of an extensive record of membrane protein structures by SS NMR, it is difficult to assess the estimated precision for the 1MAG structure and, by implication, the differences between the PDB:1MAG and 1JNO structures.

Though the general agreement among the reported PDB structures 1MAG and 1JNO is comforting, the differences are likely to have significant implications for ion channel function. For example, a difference in helical pitch has consequences for the energetics of ion permeation because it affects the pore radius and the positions of the backbone carbonyl oxygens that solvate cations as they move through the pore. Indeed, a simple calculation indicates that the energy profile of the ion passing through the PDB:1MAG and PDB:1JNO structures can differ by as much as 6 kcal/mol. Furthermore, there is a wealth of information about the effects of side chain modifications on ion permeation.[29−31] In particular substitution of Trp by the nonpolar Phe can alter the channel conductance and lifetime.[30] In addition, the Trp side chains are known to be important for the channel formation, stability, and even structure.[25,32−34] A simple calculation with a molecular mechanical force field suggests that changes in the rotameric states of Trp 9 can give rise to energy differences on the order of 1 kcal/mol for an ion in the pore. Despite the stability of the gA channel, in the sense that there usually exists a single conducting state,[35] the proximity of the pore to the surroundings means that its behavior could be very sensitive to small changes in the environment.[36] It thus becomes important to know not only the correct backbone structure but also the precise orientation of the Trp side chains because the rate of ion movement through the channel depends on the energetics of the ion-side-chain and ion-backbone interactions, and a mere 1.3 kcal/mol difference in overall interaction energy could result in a 10-fold change in ion flux.

Real understanding of ion permeation through the gA channel, which remains the best characterized ion channel,[37,38] thus hinges upon resolving the small, but extremely significant, discrepancies between the reported NMR deduced structures of gA. Resolving these questions about the structure of the gA channel will enable us to investigate important aspects of ion permeation, with relevance to a whole class of cation selective channels.[39] Furthermore, resolving these issues in the case of gA also will help clarify the significance of the orientational restraints corresponding to the observed SS NMR properties and how to best use SS NMR to extract information about the structure of membrane proteins. In particular, since the SS NMR data were measured with gA embedded in an oriented lipid bilayer, a dynamic liquid-crystalline environment, it is likely to be important to account rigorously for the influence of motional averaging. In the present paper, we attempt to resolve these uncertainties by molecular dynamics (MD) simulations of the 1MAG and 1JNO structures in DMPC lipid bilayers to quantify their relative stabilities and ability to reproduce NMR observables.

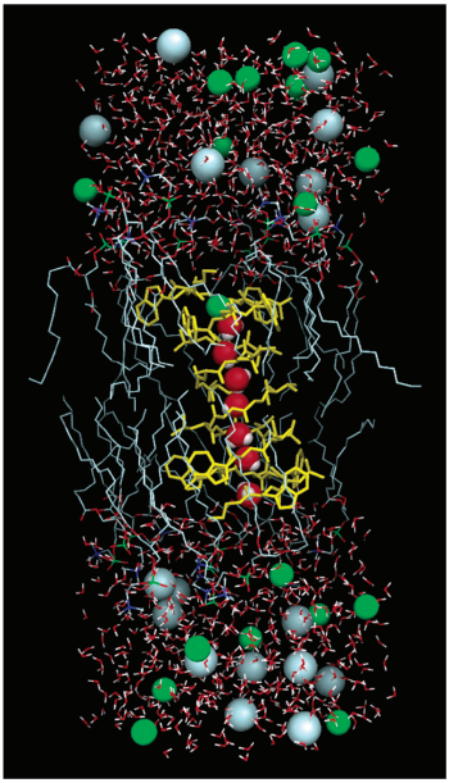

Figure 2. Microscopic simulation system: the simulation system is displayed with C, O, N and P atoms of DMPC molecules shown as gray, red, blue, and green sticks, the gA dimer as yellow sticks, K^+ and Cl^- ions as green and gray spheres, and water molecules as red (O) and white (H) sticks, except within the channel where a string of seven water molecules are displayed with their van der Waals radii.

Theory and Methods

The simulation system (Figure 2) is designed to approximate the oriented samples used in SS NMR experiments.[4] Each system consists of a gA helical dimer, 20 DMPC molecules, ~1070 water molecules, and between 19 and 20 K−Cl pairs corresponding to 1 M KCl. The total number of atoms in the primary cell is ~6180. The membrane building procedure is an extension of that previously used.[40] The system fits within hexagonal periodic boundaries with fixed sides of 32.1 Å and an initial length of ~70 Å which is allowed to vary in the *z*-direction by means of an Andersen constant pressure algorithm[41,42] with a piston weight of 750 amu. Similarly, the temperature is maintained at 330 K by means of the Nose−Hoover constant temperature algorithm[43,44] with a 3000 kcal ps^2 coupling.

(29) Durkin, J. T.; Koeppe, R. E., II; Andersen, O. S. *J. Mol. Biol.* **1990**, *211*, 221−234.
(30) Becker, M. D.; Greathouse, D. V.; Koeppe, R. E.; Andersen, O. S. *Biochemistry* **1991**, *30*, 8830−8839.
(31) Andersen, O. S.; Greathouse, D. V.; Providence, L. L.; Becker, M. D.; Koeppe, R. E., II. *J. Am. Chem. Soc.* **1998**, *120*, 5142−5146.
(32) Durkin, J. T.; Providence, L. L.; Koeppe, R. E., II; Andersen, O. S. *Biophys. J.* **1992**, *62*, 145−159.
(33) Zhang, Z.; Pascal, S. M.; Cross, T. A. *Biochemistry* **1992**, *31*, 8822−8828.
(34) Busath, D. D.; Thulin, C. D.; Hendershot, R. W.; Phillips, L. R.; Maughan, P.; Cole, C. D.; Bingham, N. C.; Morrison, S.; Baird, L. C.; Hendershot, R. J.; Cotten, M.; Cross, T. A. *Biophys. J.* **1998**, *75*, 2830−2844.
(35) Sawyer, D. B.; Koeppe, R. E., II; Andersen, O. S. *Biochemistry* **1989**, *28*, 6571−6583.
(36) Girshman, J.; Greathouse, D. V.; Koeppe, R. E., II; Andersen, O. S. *Biophys. J.* **1997**, *73*, 1310−1319.
(37) Andersen, O. S.; Koeppe, R. E. *Physiol. Rev.* **1992**, *72*, 89−158.
(38) Busath, D. D. *Annu. Rev. Physiol.* **1993**, *55*, 473−501.
(39) Doyle, D. A.; Cabral, J. M.; Pfuetzner, R. A.; Kuo, A.; Gulbis, J. M.; Cohen, S. L.; Chait, B. T.; MacKinnon, R. *Science* **1998**, *280*, 69−77.
(40) Woolf, T. B.; Roux, B. *Proteins* **1996**, *24*, 92−114. Woolf, T. B.; Roux, B. *Proc. Natl. Acad. Sci. (USA)* **1994**, *91*, 11631−11635.
(41) Andersen, H. C. *J. Chem. Phys.* **1980**, *72*, 2384−2393.
(42) Feller, S. E.; Zhang, Y. H.; Pastor, R. W.; Brooks, B. R. *J. Chem. Phys.* **1995**, *103*, 4613−4621.
(43) Nosé, S.; Klein, M. L. *Mol. Phys.* **1983**, *50*, 1055−1076.
(44) Hoover, W. G. *Phys. Rev. A.* **1985**, *31*, 1695−1697.

All simulations are carried out with CHARMM v.29[45] and the PARAM27 force field.[46] Standard parameters of DMPC molecules,[47] TIP3P water,[48] and ions[49] are used, and all bonds involving H atoms are constrained with SHAKE.[50] Electrostatic interactions are computed with the particle-mesh Ewald algorithm[51] using a Fourier spacing of 1 Å, B-spline interpolation of order 6, and real space Gaussian width of $\kappa = 0.34$ Å^{-1}, whereas Lennard−Jones interactions are truncated at 10 Å. A time step of 2 fs is employed, and trajectory data are written at 0.2 ps intervals.

Starting with each PDB structure, we carried out five simulations for a minimum of 5 ns each to obtain good statistical averaging. While the duration of each simulation is not predetermined, the total simulation time for each structure is 47 ns. Each simulation begins with a separate membrane build to explore different initial lipid distributions around the channel. Starting with the PDB:1JNO structure, we performed simulations (referred to as MD:1JNO) of lengths 5, 5, 11, 11, and 15 ns, following ∼0.5 ns of equilibration. Similarly, simulation times with the PDB:1MAG structure (referred to as MD:1MAG) are 5, 9, 9, 12, and 12 ns. Simulation times play no role in the SS NMR calculations to be reported, as each configuration is counted with equal weight in the final averages. Calculations performed on the single initial structures shall be referred to as PDB:1JNO or PDB:1MAG, while calculations from MD simulations that initiated with these structures shall be referred to as MD:1JNO and MD:1MAG, respectively.

The adiabatic energy map of the Trp side chain configurations is calculated in a vacuum by constraining the χ_1 ($N,C_\alpha,C_\beta,C_\gamma$) and χ_2 ($C_\alpha,C_\beta,C_\gamma,C_{\delta 1}$) Trp dihedral angles in one monomer with harmonic restraints of 0.3 kcal/mol/deg^2 at values from 0° to 360° in 10° increments. Backbone and side chains are restrained with force constants of 2 kcal/mol/Å^2, during 200 adaptive basis Newton−Raphson minimization steps for each (χ_1,χ_2) pair. We also estimate the relative stabilities of the different rotameric conformers of Trp 9 within the membrane environment by calculating 1D potentials of mean force (PMF), $W(\chi_1)$ and $W(\chi_2)$, connecting the rotamers of Trp 9, using umbrella sampling.[52] The 1D PMF $W(\chi_1)$, for example, is obtained by integrating out the coordinate χ_2 from the 2D PMF $W(\chi_1,\chi_2)$. A set of harmonic potentials, with a force constant of 0.06 kcal/mol/deg^2, constrain the side chain in the vicinity of each window of width $\Delta\chi_1 = 10°$, while χ_2 is maintained by applying a force constant of 0.06 kcal/mol/deg^2 when the dihedral is > 30° from the desired value. Integrating over more than 60° in the second dihedral means that the precise choice of reaction coordinate is noncritical and inaccuracies in the positions of local minima in the vacuum energy map will not impact on the PMFs. These distributions are unbiased using the weighted histogram analysis method[53,54] to produce the PMFs. Initial samples for each window are obtained from a 1 ns MD trajectory in which a transition is observed, leading to similar lipid and electrolyte distributions for every window. Because of the likely differences in lipid arrangements in equilibrated 1JNO and 1MAG structures, we perform PMFs starting with configurations sampled during transitions in each of these simulations. Each window is subject to minimization, at least 120 ps of equilibration and 500 ps of simulation during which dihedrals are written every 2 fs.

To test how each structure reproduces experimental SS NMR spectroscopy,[4] we calculate time-averaged observables for the backbone and side chains. The ^{15}N chemical shift (CS) parallel to the magnetic field (z-axis) is calculated using existing techniques,[40] with principal axes and a static CS tensor from SS NMR.[55−57] CS amplitudes are computed for both backbone and side chains. The time averaged backbone and Trp side chain $^{15}N-^{1}H$ dipolar coupling (DC) values are calculated using a standard frequency splitting of 25 kHz,[40] while backbone $^{15}N-^{13}C$ DC values are found with a standard frequency splitting of 2.3 kHz to best match all calculations with experiment. Carbon-bonded deuterium quadrupolar splitting (DQS) values are also calculated[40] with a coupling constant within indole rings of 274.5 kHz.[58] For the backbone, $C_\alpha-^{2}H$ DQS is scaled down by ∼11% to best match experiment. The present analysis necessarily relies on simplifying assumptions to enable the calculation of time-averaged SS NMR properties from a classical MD trajectory. For example, the orientation and magnitude of the chemical shift tensors are assumed to be simply attached to the local molecular moieties. In addition, the calculated DQS might be sensitive to the detailed indole ring geometry, as shown by a recent study.[59] Nevertheless the present treatment should be sufficient to capture the dominant effects of thermal fluctuations on the SS NMR properties.

These NMR observables for the backbone and Trp side chains also are computed for the PDB structures 1JNO and 1MAG. Local motional averaging of the side chain orientations is achieved by averaging over the χ_2 Trp dihedral angle only, replicating the procedure used during the optimization of the PDB:1MAG structure.[60] We generate 10^4 configurations of each Trp from Gaussian distributions centered on the PDB χ_2 value, with standard deviations ranging from 0° to 30°. Average CS, DC, and DQS are then calculated for each distribution. We find that PDB:1MAG Trp 9, 11, 13, and 15 require 15, 20, 20 and 20° Gaussian motional averagings in order to best match experimental observations. This extent of motion is consistent with the estimates of Hu et al..[60] Agreement with experiment without this treatment of local motional averaging is considerably worse for both PDB:1MAG and PDB:1JNO structures.

Results and Discussion

Backbone. The best measure of the accuracy of the 3D channel structures is its ability to reproduce the observed SS NMR observables. Results for the CS for ^{15}N sites, $^{15}N-^{1}H$ and $^{15}N-^{13}C$ DC, and $C_\alpha-^{2}H$ DQS for the backbone are displayed in Figures 3−5, respectively, obtained from the first 1 ns of each simulation, which is sufficient to obtain good statistical averages. In this period, no Trp side chain isomerizations are observed which, as part of the relaxation process, could influence the backbone structure.

As expected, prior to MD simulation, PDB:1MAG accurately reproduces the experimental values, with RMS errors in CS, $^{15}N-^{1}H$ DC, $^{15}N-^{13}C$ DC, and DQS of 5.0 ppm, 2.4, 0.24, and 18.3 kHz, respectively, as compared to 14.9 ppm, 4.5, 0.38, and 35.8 kHz, respectively, for the PDB:1JNO structure. The NMR properties for the two different PDB structures differ by

(45) Brooks, B. R.; Bruccoleri, R. E.; Olafson, B. D.; States, D. J.; Swaminathan, S.; Karplus, M. *J. Comput. Chem.* **1983**, *4*, 187−217.
(46) MacKerell, A. D., Jr.; Bashford, D.; Bellott, M.; Dunbrack, R. L., Jr.; Evanseck, J. D.; Field, M. J.; Fischer, S.; Gao, J.; Ha, S.; Joseph-McCarthy, D.; Kuchnir, L.; Kucera, K.; Lau, F. T. K.; Mattos, C.; Michnick, S.; Ngo, Y.; Nguyen, D. T.; Prodhom, B.; Reiher, W. E., III; Roux, B.; Schlenkrich, M.; Smith, J. C.; Stote, R.; Straub, J.; Watanabe, M.; Wiórkiewicz-Kuczera, J.; Yin, D.; Karplus, M. *J. Phys. Chem. B* **1998**, *102*, 3586−3616.
(47) Schlenkrich, M. J.; Brickman, J., Jr.; MacKerell, A. D.; Karplus, M. In *Biological Membranes. A molecular perspective from computation and experiment*; Merz, K. M., Roux, B., Eds. Birkhauser: Boston, MA, 1996; pp 31−81.
(48) Jorgensen, W. L.; Chandrasekhar, J.; Madura, J. D.; Impey, R. W.; Klein, M. L. *J. Chem. Phys.* **1983**, *79*, 926−935.
(49) Beglov, D.; Roux, B. *J. Chem. Phys.* **1994**, *100*, 9050−9063.
(50) Gunsteren, W. F.; Berendsen, H. J. C. *Mol. Phys.* **1977**, *34*, 1311−1327.
(51) Darden, T.; York, D.; Pedersen, L. *J. Chem. Phys.* **1993**, *98*, 10089−10092.
(52) Torrie, G. M.; Valleau, J. P. *J. Comput. Phys.* **1977**, *23*, 187−199.
(53) Kumar, S.; Bouzida, D.; Swensen, R. H.; Kollman, P. A.; Rosenberg, J. M. *J. Comput. Chem.* **1992**, *13*, 1011−1021.
(54) Souaille, M.; Roux, B. *Comput. Phys. Commun.* **2001**, *135*, 40−57.
(55) Hu, W.; Lee, K. C.; Cross, T. A. *Biochemistry* **1993**, *32*, 7035−7047.
(56) Nicholson, L. K.; Cross, T. A. *Biochemistry* **1989**, *28*, 9379−9385.
(57) Teng, Q.; Cross, T. A. *J. Magn. Reson.* **1989**, *85*, 439−447.
(58) Roux, B.; Woolf, T. B. In *Human to Proteins, Advances in computational life sciences* 2; Michalewicz, M. T., Ed. CSIRO Publishing: Australia, 1998; pp 183−200.
(59) Koeppe, R. E., II; Sun, H.; van der Wel, P. C. A.; Scherer, E. M. Combined Experimental/Theoretical Approach to Indole Ring Geometry using Deuterium Magnetic Resonance and ab initio Calculations. *J. Am. Chem. Soc.*, submitted March 2003.
(60) Hu, W.; Cross, T. A. *Biochemistry* **1995**, *34*, 14147−14155.

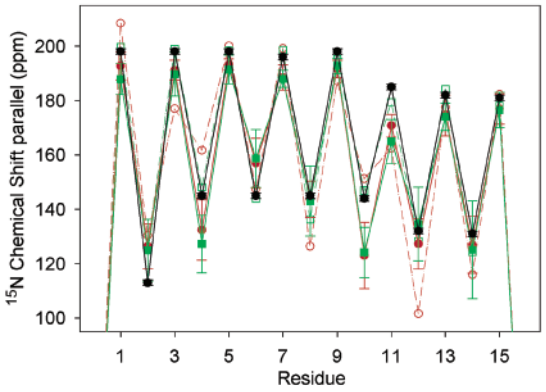

Figure 3. Backbone SS NMR CS: The ^{15}N CS parallel to the membrane normal is plotted against residue number. Experimental values (Cross, T. A., personal communication) are plotted as black squares with error bars. The CS values calculated for the PDB:1JNO structure are shown as open red circles and dash−dot lines; the values for the PDB:1MAG structure are shown as open green squares and dash−dot lines. The average CS results from MD:1JNO are shown as solid red circles, solid lines, and error bars (standard deviation from five simulations), while average MD results for MD:1MAG are shown as solid green squares, solid lines, and error bars. These symbols, lines, and colors will be used throughout the paper. Each point is an average of five simulations of two monomers taken from the first 1 ns of each simulation.

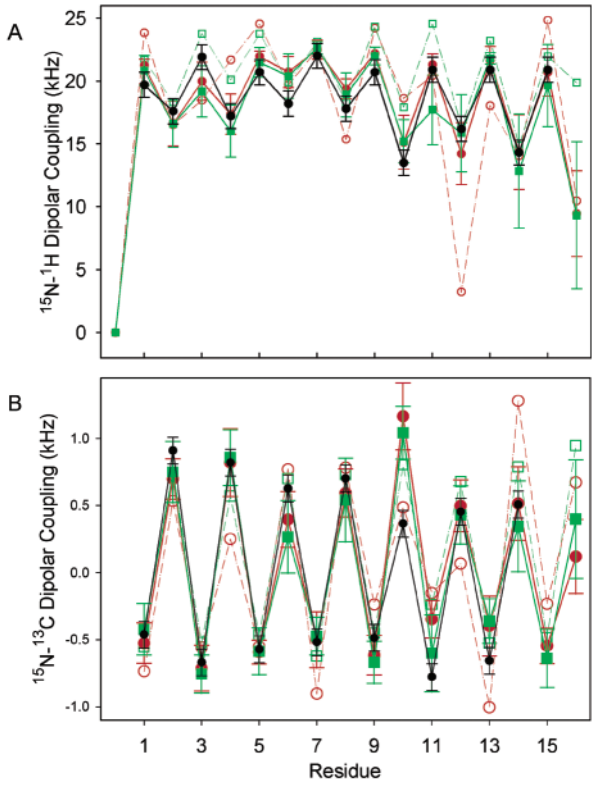

Figure 4. Backbone SS NMR DC: (A) the ^{15}N−^{1}H (A) and ^{15}N−^{13}C (B) DC are plotted against residue number using the same notation as that in Figure 3, obtained with the same procedure.

11.8 ppm, 4.3, 0.28, and 28.8 kHz, respectively, and appear significantly different in Figures 3−5.

The PDB:1JNO and PDB:1MAG backbones differ structurally, as indicated by the results of the NMR calculations. The PDB:1JNO backbone has 6.3 residues and a 4.7 Å rise per turn, which is in good agreement with X-ray scattering,[61] while the PDB:1MAG backbone has 6.5 residues and a 5.1 Å rise per turn. In addition, the energy of the PDB:1JNO and PDB:1MAG

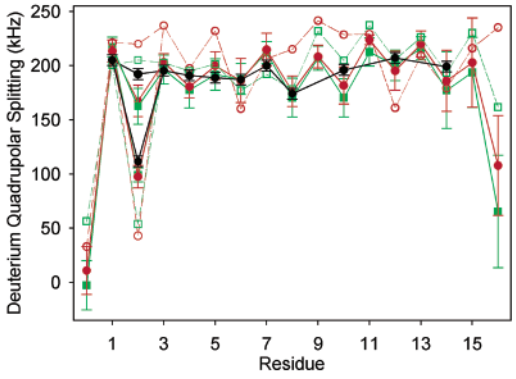

Figure 5. Backbone SS NMR DQS: The $C_\alpha-^{2}H$ DQS is plotted against residue number using the same notation as in Figure 3, obtained with the same procedure. The two values for residue 2 correspond to the two H_α's on the Gly residue.

Table 1. Energy Components for Initial PDB Structures 1JNO and 1MAG[a]

	backbone		side chains		complete gA	
energy	1JNO	1MAG	1JNO	1MAG	1JNO	1MAG
bond	39	726	50	864	93	1594
angle	39	65	43	157	107	838
dihedral	24	39	8	31	134	176
vdW	−47	5	−3	31	−142	23
electrostatic	68	94	−60	−66	109	111
total	122	929	38	1017	302	2742
force	8	58	11	56	10	63

[a] Bond, angle (including Urey−Bradley), dihedral (including improper dihedral), van der Waals, electrostatic, total energy (kcal/mol), and RMS force (kcal/mol/Å) are shown for PDB:1JNO and PDB:1MAG Structures. Energies are listed for the 198 backbone atoms (N, H, C_α, carbonyl C and O atoms), the 354 side chain atoms (all nonbackbone atoms), and the complete gA dimer. Note, when calculating individual backbone or side chain energies, no interaction between backbone and side chains included, and their sum will not equal the result for the complete gA dimer.

static structures in vacuum, listed with the various contributions in Table 1, reveals considerable strain in both the PDB:1MAG backbone and side chains; the majority of the strain being in the bond and angle energy terms. By carrying out MD simulations, starting with the PDB structures, we find it is possible to relax these energy strains and to account for the complex molecular motions that play a major role in the calculation of SS NMR observables. We calculate time-averaged CS, DC, and DQS for the backbone from the MD:1JNO and MD:1MAG simulations, also plotted in Figures 3−5. For both simulations, the results are in good agreement with experimental data, being favorably comparable to PDB:1MAG. Only the CS and ^{15}N−^{13}C DC of residue 10 exhibit noticeable deviations from experiment, this being the residue for which PDB:1MAG also fits the data less well. The RMS errors in CS, ^{15}N−^{1}H DC, ^{15}N−^{13}C DC, and DQS are 9.8 ppm, 1.3, 0.27, and 12.6 kHz, respectively, for MD:1JNO and 11.2 ppm, 1.6, 0.24, and 15.0 kHz for MD:1MAG. The results from MD:1JNO and MD:1MAG are, in fact, very similar with deviations between the two structures of only 3.2 ppm, 1.2, 0.10, and 12.5 kHz in CS, ^{15}N−^{1}H DC, ^{15}N−^{13}C DC, and DQS, respectively, a factor 3 to 4 less than the deviations between the initial PDB structures.

The average number of residues and axial rise per turn in the MD:1JNO simulations are 6.25 ± 0.04 and 4.84 ± 0.07 Å,

(61) Katsaras, J.; Prosser, R. S.; Stinson, R. H.; Davis, J. H. *Biophys. J.* **1992**, *61*, 827−830.

respectively, while the corresponding averages for MD:1MAG are 6.24 ± 0.03 and 4.87 ± 0.11 Å, respectively. For both MD averaged structures, the axial rise is in good agreement with the value determined by X-ray scattering of 4.7 ± 0.2 Å.[61] Significant change in the PDB:1MAG backbone structure is required to decrease the helical pitch to match this value. In fact, the RMS deviation of the average structure from MD (obtained from the first 1 ns of all simulations) relative to the PDB structure for 1MAG (0.95 Å) is much higher than that for 1JNO (0.63 Å). Moreover, the 1MAG structure is changing further during the simulations, with the average structure from MD over the last 1 ns of all simulations deviating relative to the PDB:1MAG structure by 1.20 Å, whereas the deviation for 1JNO remains at 0.63 Å.

The RMS deviation between PDB:1JNO and PDB:1MAG backbones of 1.4 Å decreases to 0.36 Å for the MD-averaged structures from the first 1 ns of all MD:1JNO and MD:1MAG simulations and to only 0.21 Å for the average structures obtained from the last 1 ns of simulation. Nevertheless, during the first 1 ns of simulation, the variation among the instantaneous structures within the MD:1MAG simulation (RMS deviation 1.4 Å) remains higher than that of the MD:1JNO simulations (0.8 Å). This greater variation in the backbone structure within the MD:1MAG simulations indicates that some backbone stress is maintained during this early period of simulation. Consistent with this interpretation, the variation among the instantaneous structures from the last 1 ns of each simulation decreases to ~0.7 A in both MD:1JNO and MD:1MAG simulations. The fact that several ns of relaxation is required to remove the stresses within PDB:1MAG, while the NMR observables and helix pitches converge quickly, suggests that this backbone stress could be associated with particular side chain orientations, which undergo transitions on a longer (multinanosecond) time scale. While Val side chains occur in the same rotameric states in PDB:1JNO and PDB:1MAG structures, there are differences in the Leu side chain orientations. The Leu side chains undergo frequent isomerizations during both MD:1JNO and MD:1MAG simulations, suggesting that they are not responsible for the stressed backbone of PDB:1MAG. In contrast, Trp 9 maintains a different rotameric state in each simulation for periods of many nanoseconds and sometimes during the entire simulation. This again emphasizes the need to understand the significance of the difference in Trp 9 side chain orientation.

Trp Side Chains. A simple adiabatic energy map (Figure 6) can serve as a guide to the accessible configurations of the Trp 9 side chain. The T rotamer observed in the PDB:1JNO structure and the K rotamer observed in PDB:1MAG structure are within 1 kcal/mol of each other, contrary to the suggestion that the 1MAG structure has a large repulsive stacking interaction of the Trp 9 and Trp 15 (cf. ref 21). Figure 6 shows that all six possible rotamers for Trp residues[62] are discernible, but only four are likely to be occupied. These four rotameric states are common to all gA Trp side chains in SS NMR.[4,22] However, the vacuum energy maps of Trp 11 and 15 (not shown) have five of the six rotamers within 2 kcal/mol of the lowest energy rotamer. According to a rotamer library based on a sample of 325 proteins,[62] neither the T rotamer of PDB:1JNO nor the K rotamer of PDB:1MAG is among the most frequently observed. (In proteins, the relative populations of Trp side chains are 12%, 13%, 19%, and 39% for the T, K, TK1, and TK2 rotamers, respectively.) This is not surprising because both the membrane environment and the interactions with other side chains are expected to influence the preferred rotameric states of Trp 9. To address this question further, we now examine the orientation of the Trp side chains over extended MD simulations of gA embedded in a lipid bilayer.

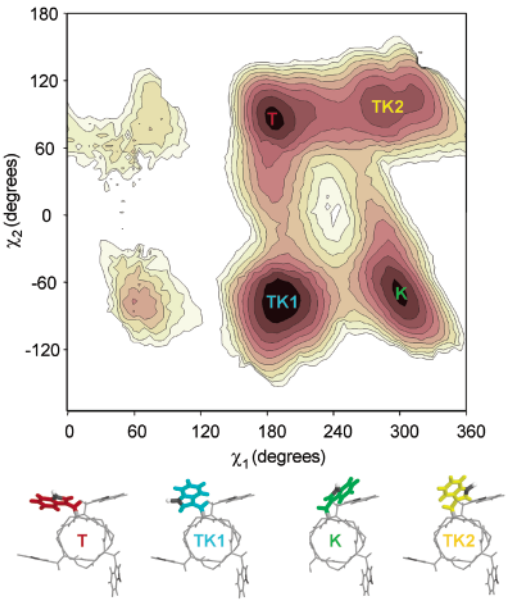

Figure 6. Adiabatic energy map of Trp 9 configurations: The map is plotted for χ_1 from 0 to 360°, and χ_2 from −180 to 180° because this allows for the most convenient display in Figure 7. Six minima can be identified, with the four lowest labeled T (corresponding to that present in PDB:1JNO of Townsley et al.[21]), K (present in PDB:1MAG of Ketchem et al.[11]), TK1, and TK2. The orientations of the Trp side chains in the four states are illustrated beneath the graph. The N−H bonds on the indole rings are drawn as black sticks with white hydrogen balls. Each color shade in the map represents 1 kcal/mol in energy. The map is generated by starting with the PDB:1JNO structure. That obtained with the PDB:1MAG structure is qualitatively similar, with the same local minima and relative energies (data not shown).

Over the entire simulation time of 0.1 μs, the rotameric states are fairly stable. In fact, Trp 11, 13, and 15 undergo just 1, 2, and 0 changes in rotameric state. Only Trp 9 is fairly mobile, undergoing 18 transitions during the same period. This may be surprising given that Trp 9 is buried deepest in the membrane, but the Trps closer to the membrane surface could be more restricted in their motions due to differences in hydrogen bond interactions with water molecules and lipid headgroups. Figure 7A shows the time evolution of the dihedral angles of Trp 9 in one monomer, where the initial structure $(\chi_1,\chi_2) \approx (190°,80°)$ corresponds to the T rotamer of PDB:1JNO (Figure 6). After 8 ns, the change in χ_2 signals a transition to the TK1 rotamer (190°, −80°), and at 10 ns, there is a second transition to the K rotamer (280°, −80°) of the PDB:1MAG structure, after which the Trp alternates between K and TK1. The trajectory in Figure 7B begins in the K rotamer and after ~7.5 ns undergoes a transition to the T rotamer. In either case, the path between T and K involves TK1, though this is more obvious in Figure 7A than in 7B. A plot of (χ_1,χ_2) is given in Figure 7C and D for all simulations MD:1JNO and MD:1MAG, respectively. There is significant interconversion between the T and K rotameric states of Trp 9, though only 3 of the 4 low-lying states are visited during these simulations. That the populations provided in Figure

(62) Dunbrack, R. L., Jr.; Karplus, M. *J. Mol. Biol.* **1992**, *230*, 543−574.

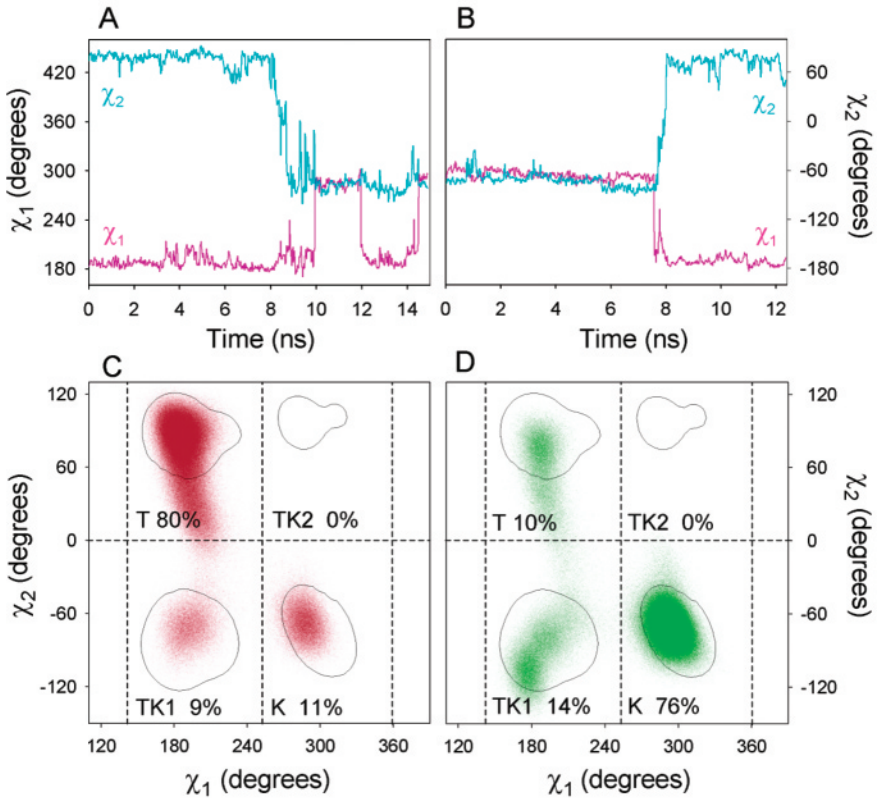

Figure 7. Side chain transitions and state populations: (A) A 15 ns trajectory of χ_1 (pink) and χ_2 (cyan) trajectories of the Trp 9 side chain in one monomer starting with the PDB:1JNO structure. Each point is a 10 ps block average. (B) A 12 ns trajectory starting with PDB:1MAG. (C,D) Scatter plots of 1 million observed (χ_1,χ_2) points from all 10 simulations starting with either the PDB:1JNO (C) or PDB:1MAG (D) structures. The solid contour denotes the lowest energy state +3 kcal/mol (cf. Figure 6). Four regions envelope the lowest lying rotameric states, divided by the dashed lines at $\chi_1 = 140°$, 250°, and 360°, and $\chi_2 = -150°$, 0°, and 150°. The percentage of time spent in each of these boxes is noted.

7C and D are not equal suggests that there is a significant barrier to moving the Trp side chain out of both the T and K states: Trp 9 spends less than 25% of the time outside its initial state.

The magnitude of the fluctuations in χ_1 and χ_2 found here is in general accord with the estimates obtained from inhomogeneous spectra taken from fast frozen oriented bilayer samples.[60] We investigate the extent of motion in the Trp 9 side chain in more detail by simulating these inhomogeneous spectra from MD simulation. This is done by generating histograms of the instantaneous values of the CS, as if all kinetic energy and thermal fluctuations were suddenly removed from the trajectory. Figure 8 shows these histograms for the CS of T, K, and TK1 states. It is evident that the inhomogeneous spectrum from fast frozen oriented samples of gA in lipid bilayers possesses a similar if not higher level of motion than does the side chain in the MD simulation.

We are now in a position to examine how well each of the observed rotameric states reproduces the experimental data. Dividing the simulations into predefined regions in Trp 9 (χ_1,χ_2) space (cf. Figure 7), we calculate average NMR quantities for the 4 Trp side chains, which we compare to the observed SS NMR and to motionally averaged NMR quantities calculated from the static PDB structures (1MAG and 1JNO). NMR results for the Trp side chains are shown in Figures 9 and 10. In the case of the CS (Figure 9A), whether Trp 9 is in the T or K rotameric state, there is broad agreement of MD averages with experiment for all Trp side chains. Also, in the case of the DC (Figure 9B), there is broad agreement between MD averages and experiment for all Trp's, except for Trp 9 in the K state,

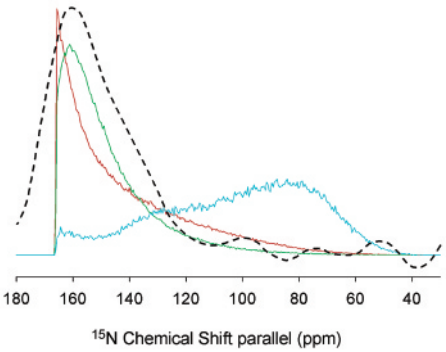

Figure 8. CS inhomogeneous spectrum: The histogram of the instantaneous values of the Trp 9 ^{15}N CS parallel to the membrane normal is plotted for the three predominantly occurring rotameric states of Trp 9 identified in Figure 7. Following the color scheme of Figure 6, the spectrum for the T state is shown in red, K state, in green, and the TK1 state, in cyan. The experimental spectrum (see Figure 7B of ref 60) has been reproduced with a dashed black line fit, with adjusted amplitude. Each spectrum is generated from analysis of all 10 simulations of 2 gA monomers.

which exhibits a fairly large deviation. A similar observation can be made from the DQS calculations for the five deuterium-labeled sites on each Trp (Figure 10). While the MD averaged DQS for Trp 11, 13, and 15 are in good agreement with experiment for both the T and K rotamers, there are important differences in the case of Trp 9. The DQS MD averages for Trp 9 in the T state lead to excellent agreement for Trp 9 (RMS deviation 23.2 kHz). In contrast, the results for the K rotamer are significantly worse for all five sites (RMS deviation 74.6 kHz). Even though Trp 9 remains in the energy well corre-

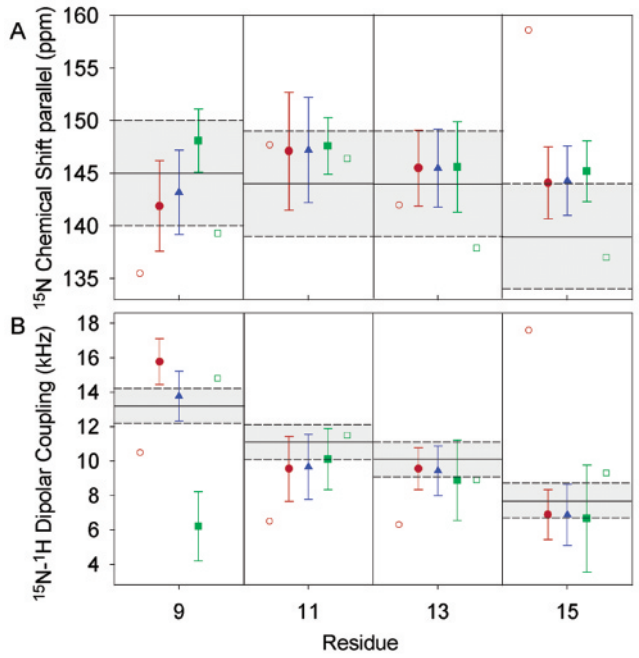

Figure 9. Side chain SS NMR CS and DC: (A) The ^{15}N CS parallel to the membrane normal for each Trp. Experimental values (Cross, T. A., personal communication) are plotted as black horizontal solid lines, with dashed shaded boxes indicating the error bars for each value. Following the same scheme as in Figures 3, 4, and 5, the CS values calculated for the PDB:1JNO structure, following Gaussian averaging (see Theory and Methods), are shown as open red circles, while values for the PDB:1MAG structure are shown as open green squares. Average CS values from MD with Trp 9 in the T state, identified in Figure 7, are shown as solid red circles and error bars, while average MD results for the K rotameric state are shown as solid green squares with error bars. The least squares mix of states (see text) is plotted as blue triangles with error bars. (B) The ^{15}N−^{1}H DC for each Trp is plotted for experimental, PDB, and MD averages using the scheme in part A.

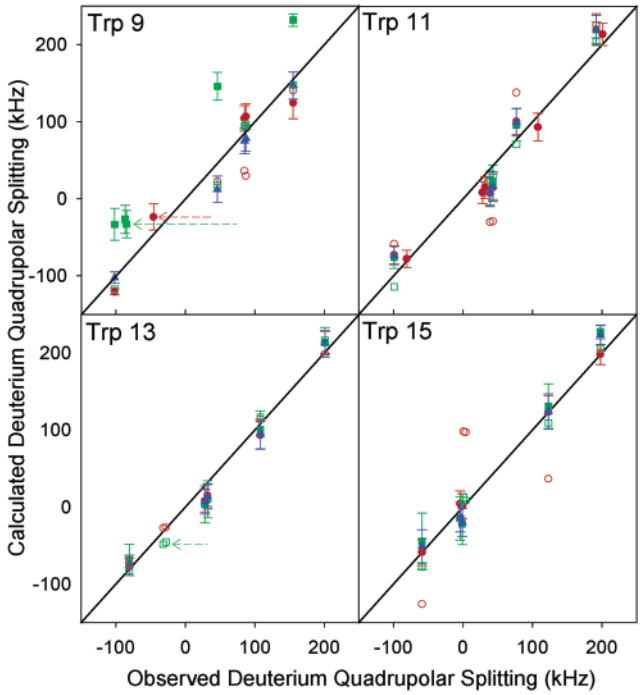

Figure 10. Side chain SS NMR DQS: The DQS of the five deuterium labeled sites on each Trp side chain are plotted against the observed values (Cross, T. A., personal communication); the black diagonal line denotes experimental values (identity), while the same color scheme as in Figure 9 is used for PDB and MD calculations. The δ_1 observed splitting on Trp 9 is changed from +46 to −46 kHz (see text) for the T rotameric state (red arrow). For the K state, the sign reversals are η_3 from +87 to −87 kHz and ζ_2 from +85 to −85 kHz (see text) in Trp 9 (green arrow). The sign reversals for DQS corresponding to sites η_3 and ζ_2 of PDB:1MAG Trp 13 (open green squares) are indicated by a single green arrow. No sign reversals are required for the empirical mix results (blue triangles).

sponding to the K rotameric state (cf. Figure 6) during the trajectory of MD:1MAG, the side chain adopts an orientation that yields calculated SS NMR properties that are in clear disagreement with the experimental observations. This shows that the K rotameric state cannot be the dominant rotameric state in lipid bilayers. In contrast, the T rotameric state after MD relaxation leads to a side chain orientation that provides good agreement with this SS NMR data. Correspondingly, the solution NMR NOESY distance constraints involving Trp 9[21] are described better by averages calculated from MD based on the T rotamer (RMS error 1.2 Å) than on the K rotamer (RMS error 2.3 Å). Thus, following equilibration of the structures in the DMPC bilayer, only the side chain orientation of Trp 9 present in PDB:1JNO can broadly reproduce experimental SS and solution NMR observables: the PDB:1MAG structure is unable to provide satisfactory agreement with either experiment.

Particular difficulties are encountered in assessing the agreement of structural models with the observed DQS. Because the DQS experiments were performed with perdeuterated Trp side chains, the assignment to specific sites is not straightforward, and different assignments were reported by Ketchem et al.[4] and Koeppe et al..[22] Furthermore, the DQS amplitudes range from −137 to +274 kHz,[40] but only their absolute magnitudes are measurable. Therefore, the sign of any observed DQS with a modulus < 137 kHz (all sites except ζ_3) is undetermined. In such cases, one must seek which value, positive or negative, yields the better agreement, consistent with a structural model. We find that attributing negative values to one or two MD averaged DQS values, based on a single rotameric state (T or K) for Trp 9 (cf. Figure 10), yields the best agreement with SS NMR.

Results for PDB structures with Gaussian averaging (see Theory and Methods) are also included in Figures 9 and 10. Not surprisingly, the results based on PDB:1MAG are in better agreement than those based on PDB:1JNO, which has a particularly large disagreement for the CS and DC for Trp 15. The disagreement for the Trp 15 of PDB:1JNO, which is obvious in the CS, DC, and DQS of Figures 9 and 10, might be a consequence of a difference in the environment at the surface of a detergent micelle compared with that of a phospholipid bilayer membrane. Remarkably, the MD trajectory leads to a very small change in the orientation of Trp 15 relative to PDB:1JNO, but this is sufficient to yield an excellent agreement with all SS NMR observables for this side chain. The DQS from the PDB:1MAG structure are in excellent agreement with experiment, while those from PDB:1JNO are in noticeably poorer agreement for Trp 9, 11, and 15. The ability of MD simulations to improve the calculated CS, DC, and DQS of the 1JNO structure is particularly striking, as all the values converge toward the SS NMR observation, most noticeably for Trp 15. While MD simulation within the K state also provides improved results with respect to calculations based on PDB:1MAG, the incorrect values obtained for Trp 9 are consequences of that rotameric state. Interestingly, the MD averages for Trp 9 in the T rotameric state reproduce the experi-

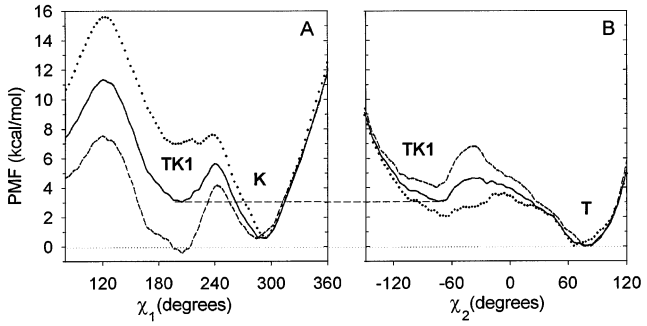

Figure 11. Potential of mean force of the Trp 9 side chain: (A) The PMF of Trp 9 in one monomer from umbrella sampling along the χ_1 coordinate from 150° to 350° with χ_2 constrained near −80°. (B) The χ_2 PMF from −150° to 150°, with χ_1 near 190°. The dashed curves represent the PMFs obtained with starting configurations from a T → K transition in an MD: 1JNO simulation, the dotted curves are the PMFs from a K → T transition in an MD:1MAG simulation, and the solid curves are the PMFs obtained from all windows. Results are offset such that the Townsley (T) state has the energy 0 kcal/mol and such that the TK1 state has the same energy in each PMF.

mentally observed downward trend of the DC with residue number, a trend that arises from an increased alignment of the N−H vector with the membrane normal for side chains deeper into the membrane. The agreement originally seen in PDB:1MAG is lost in MD:1MAG when the structure is freely relaxed during the trajectory because the Trp 9 N−H dipole assumes a different orientation, though the ring remains in the K rotameric state.

The observation of spontaneous isomerization in several of the MD simulations suggests that gA in the lipid bilayer is best represented by a superposition of rotameric states of Trp 9. Using an empirical least-squares fit to obtain the best agreement with all available SS NMR data leads to a mixture of states with 80% T, 20% K and no TK1 or TK2. The site assignments and optimal signs for the DQS determined for this 4:1 mix of T and K states, supports those previously reported by Ketchem et al..[4] The resulting NMR quantities for this mixed state (blue triangles in Figures 9 and 10) exhibit reduced deviations from observed values for the DQS of Trp 9 (RMS error 16.2 kHz); the deviations in CS and DC also have been decreased from those of the pure T state. For all other Trp residues, the DQS RMS deviation is now just 18.9 kHz, and CS and DC errors are reduced or maintained.

Although the agreement between calculated and observed NMR properties is excellent for this mixture of states, one might question the significance of such empirically determined populations of rotameric states. Ideally, the population should arise spontaneously from long MD trajectories. Isomerizations occur only infrequently; however, and a direct brute force approach is computationally prohibitive. To address concerns about the relative populations of the rotameric states in the membrane environment, we calculate the PMF along the reaction coordinate χ_1, linking TK1 and K, and along χ_2, linking TK1 and T (Figure 11). It is evident that the local energy minima that are observed in the adiabatic vacuum energy map shown in Figure 6 also exist in these PMFs obtained by MD simulation in the presence of the membrane environment. The lowest energy state can be identified as the T rotamer, and the three states are separated by barriers of 4−6 kcal/mol. The next lowest lying state is K, being 0.6 kcal/mol higher in energy, followed by TK1 which is 2.5 kcal/mol above the K state. This analysis reinforces the observation that the occupancy of the TK1 rotamer is low, its inclusion causing further deviation from experimental SS NMR observations. Indeed, inspection of Figure 8 shows that the TK1 rotamer is occupied only a small fraction of the time; otherwise its presence would be evident in the shape of the experimental spectrum. Although the relative stability of the rotamers calculated from the PMFs is broadly consistent with the results suggested by the empirical least-squares fitting procedure, the dependence upon the initial starting configurations suggests that there is considerable uncertainty in these estimates. This presumably is a consequence of the difficulties in sampling lipid configurations, even with multinanosecond simulations, and reinforces the importance of the SS NMR observables to identify the dominant configurations in the bilayer.

Finally, we note that the partial quenching observed in Trp fluorescence spectroscopy[23,24] suggests that some stacking of indole rings is occurring on the time scale of the fluorescent decays (ranging from 0.4 to 8.8 ns). Such stacking is not present in the dominant T state but is present in the K state. Kramer's transition rates can be calculated from the biased PMF time series of dihedrals in the high friction, large activation regime, using the procedure described in ref 63. The transition rate between two stable states is given approximately by the expression

$$k = \frac{D(\chi_b)}{2\pi k_B T}[-W''(\chi_b)W''(\chi_w)]^{1/2} e^{\Delta W^{\ddagger}/k_B T} \qquad (1)$$

where $D(\chi_b)$ is the diffusion constant measured near the top of the barrier, as calculated using the generalized Langevin equation for a harmonic oscillator, W'' is the second derivative of the PMF estimated (at the barrier χ_b and well χ_w) by harmonic fits, and $\Delta W^{\ddagger}$ is the activation barrier height for the transition. The estimated rates of the K → TK1 and TK1 → K transitions are 0.3 ns^{-1} and 10 ns^{-1}, respectively, while those for T → TK1 and TK1 → T transitions are 8 ns^{-1} and 670 ns^{-1}, respectively. These estimates are in general agreement with the unbiased simulations of Figure 7. The stacked Trp configuration in the K state occurs at a time scale that can account for the fluorescence quenching. That is, a 4:1 mixture of the T and K rotamers, interconverting on the nanosecond time scale, is compliant with both SS NMR and fluorescence spectroscopy observations.

Conclusion

An important challenge in the analysis and interpretation of SS NMR observables, for the purpose of extracting structural information, is to account for the complexities of molecular motions. This motion occurs on many levels and time scales, from the rapid localized librations of molecular moieties, to isomerizations between rotameric states, cooperative and global movements of the molecule, and finally the relaxation of the molecule toward the free energy minimum under the influence of its environment. This complexity complicates attempts at obtaining a unique refined structural model using orientational restraints from SS NMR. Our results show that the PDB:1MAG structure, with appropriate incorporation of local motional averaging, adequately reproduces NMR observations; but, the

(63) Crouzy, S.; Woolf, T. B.; Roux, B. *Biophys. J.* **1994**, *67*, 1370−1386.

structure is highly stressed because it was optimized with stringent orientational restraints, with a small weight given to the molecular mechanical energy function.[1] Additional efforts to refine PDB:1MAG,[26] such that over-fitting the structure to orientational restraints is avoided, still results in strains of a few hundred kcal/mol in the gA dimer. Importantly, the ability of a static NMR structure to reproduce experiment only becomes apparent when MD simulation is employed to relax these strains and explicitly treat the motional averaging of the protein.

A remarkably consistent picture of the conformation of gA in lipid bilayers has emerged from this study. The two major concerns at the outset were the differences in the backbone pitch and the orientations of the Trp 9 side chains in the available SS and solution NMR structures. Despite the differing helical pitches and NMR observables of the initial PDB:1JNO and PDB:1MAG structures, the two backbones become nearly indistinguishable after dynamic relaxation in the bilayer, attaining helical pitches consistent with independent X-ray determination[1] and backbone NMR observables in close agreement with experiment. The backbone of PDB:1MAG, however, requires a longer relaxation period in the bilayer, possibly a result of the particular arrangement of the side chains in that structure.

MD simulations demonstrate that the rotamer of Trp 9 present in the PDB:1MAG structure cannot be the dominant configuration within a lipid bilayer environment. While this rotameric state remains stable for up to several nanoseconds, it takes on a slightly different orientation in the relaxed structure, relative to the membrane normal, which is in sharp disagreement with SS NMR DC and DQS observables. Conversely, the Trp 9 rotamer present in the PDB:1JNO structure is shown to be more stable and to more accurately reproduce SS NMR quantities. The ability of MD to relax a PDB structure that poorly reproduces SS NMR observations and include dynamical averaging to achieve close agreement with experiment is remarkable; this is particularly noteworthy in the case of Trp 15 of PDB:1JNO (cf. Figures 9 and 10). Furthermore, the PDB:1JNO structure, relaxed in the DMPC bilayer, also matches the NOESY distances obtained from solution NMR in detergent micelles accurately. Thus, the PDB:1JNO structure approximates best the dominant configuration in both DMPC bilayer and detergent micellar environments, which implies that detergent micelles provide a good membrane mimicking medium.

The observed isomerizations of the Trp 9 side chain (Figure 7) suggest that a mixture of rotameric states may better reproduce experiment. In fact, empirical fitting, supported by umbrella sampling calculations, suggests that a mixture of states consisting of 80% T and 20% K rotamers best reproduces side chain NMR observables. The estimated interconversion rate is also consistent with fluorescence spectroscopic observations. A single rotameric state would be unable to account for all of these experimental findings.

MD simulation enables one to go beyond considerations based on static structures of proteins. Microscopic models incorporating a realistic molecular environment can be used to generate a dynamic ensemble that reproduces experimental observations with remarkable precision. MD simulations have been used to account for conflicting information from different experiments, leading to a refined understanding of the structure of the gA channel in lipid membranes, thus demonstrating that this approach can be a powerful tool for structural refinement of other membrane proteins.

Acknowledgment. This work was supported by the Keck Foundation (T.W.A.) and NIH Grants GM21342 (O.S.A.) and GM62342 (B.R.). The authors thank Dr. Roger E. Koeppe II for insightful discussions, Dr. T. A. Cross for helpful conversation and providing experimental SS NMR observations, and Dr. J. Hinton for kindly supplying experimental NOESY constraints from solution NMR.

JA029317K